Verification of the Domains Tracking Algorithm for Solving the System of Allen-Cahn and Cahn-Hilliard Equations

Dmitry Prokhorov[1(✉)], Yaroslav Bazaikin[2], and Vadim Lisitsa[3]

[1] Institute of Petroleum Geology and Geophysics SB RAS, Koptug ave. 3, Novosibirsk 630090, Russia
prokhorovdi@ipgg.sbras.ru

[2] Faculty of Science, Jan Evangelista Purkyně University in Ústí nad Labem, Pasteurova 3632/15, Ústí nad Labem 400 96, Czech Republic
yaroslav.bazaykin@ujep.cz

[3] Sobolev Institute of Mathematics SB RAS, 4 Koptug ave., Novosibirsk 630090, Russia
lisitsavv@ipgg.sbras.ru

Abstract. The sintering process is widely used in modern industry because it allows for obtaining materials with predefined properties. Chemical or physical techniques can measure these properties. Besides the cost of such methods, it is worth noting that some techniques destroy samples, which causes difficulties in measuring the parameters' evolution. Computer simulation of the sintering process allows for overcoming these difficulties. The sintering models based on the system of Cahn-Hilliard and Allen-Cahn equations require optimization if the number of grains is large. However, optimizations affect the solution; thus, a detailed quality assessment is required. The article presents such a study for our optimization: the Allen-Cahn equations are solved in small subdomains of the whole computational domain, which change over time. We provide comparative tests between solutions obtained by our algorithm and solutions obtained by solving the system in the whole domain. Besides common approaches, we use powerful tools of topology: Hausdorff distance and Betti numbers. The choice of the algorithm parameters is justified by obtained accuracy and efficiency.

Keywords: Sintering · Phase-field · Cahn-Hilliard equation · Allen-Cahn equation

1 Introduction

Sintering is a common way to obtain a material with predefined filtration, strength, and sorptive properties. For example, tungsten and silicon carbides are widely used for extra durable tools, and abrasives [27,33]. Another example

© The Author(s), under exclusive license to Springer Nature Switzerland AG 2023
O. Gervasi et al. (Eds.): ICCSA 2023 Workshops, LNCS 14104, pp. 693–707, 2023.
https://doi.org/10.1007/978-3-031-37105-9_46

is the sintering of sorbents for the chemical adsorption of CO_2 [4,5,10]. The process of sintering a granular material with the formation of a porous structure depends on many factors, such as temperature, duration of exposure, external loads, etc., which significantly impact the properties of the resulting material on a macroscale. Thus, computer simulation of sintering is an actual problem of modern material science [6].

We can consider sintering simulation as a moving-boundary problem or Stefan problem. One of the common ways to solve such problems is the level-set method [17,18,24] combined with the immersed boundary method [21,22,25,31,34]. However, the level-set method is more applicable to the simulation of the chemical interaction between fluid and rock [15,28] or to the modeling of the multiphase fluid flows [14,36] than for the sintering simulation [26,30].

Instead of a level-set approach, the phase-field method is often used to model sintering [13,37] and related problems, such bulk phase as solidification [12] and grain growth [23]. The key feature of this method is continuous fields describing the shapes and orientations of different grains. Field variables correspond to physical quantities such as composition and order parameters. They take definite values in grains and smoothly change at the interface.

In the case of a single-component system, the model is described by one conservative Cahn-Hilliard [7] equation and by I Allen-Cahn [2] equations (Sect. 2), where I is the number of grains. Each of the Allen-Cahn equations describes the evolution of the order parameter corresponding to one of the grains [35]. Using finite difference methods for solving this system requires storing values of order parameters for each grain. Thus, increasing the number of grains with a regular grid size causes the growth of computation efforts, but order parameters take zero value on most of the grid.

One method to overcome this difficulty is described in [16]. The principle of this method is that each grid node stores values only of I_c order parameters, where I_c is a predefined constant. Authors of [16] conducted a detailed study about the influence of their algorithm on the grain growth process and determined the optimal parameter.

Similar to [16], we performed a qualitative assessment of our approach (Sect. 3), in which each of the Allen-Cahn equations is solved in a small subdomain corresponding to the current grain. However, we are interested in changes in geometry and topology of sample structure under the influence of high temperature because they are related to chemisorption and strength properties. Therefore, we use topological approaches to the comparison, such as Hausdorff distance [3] and Betti numbers [8] (Sect. 4). The testing results, including the performance, are presented in Sect. 5.

2 Problem Statement

Let us consider a rectangular domain $\Omega = [X_1^{min}, X_1^{max}] \times [X_2^{min}, X_2^{max}] \times [X_3^{min}, X_3^{max}]$. Some part of Ω is occupied by grains; the rest of Ω is called pores. Order parameters $\eta_i(\mathbf{x}, t), 1 \leq i \leq I$ describe the crystallographic orientation of

grains. They vary from 0 to 1. Parameter $\rho(\mathbf{x}, t)$ describes the mass density and varies in the same interval. For example, in Fig. 1, we can see a one-dimensional domain, where $\eta_i = 1$ in the grain i, $\eta_i = 0$ in the pore, and η_i smoothly varies between these values at the interface.

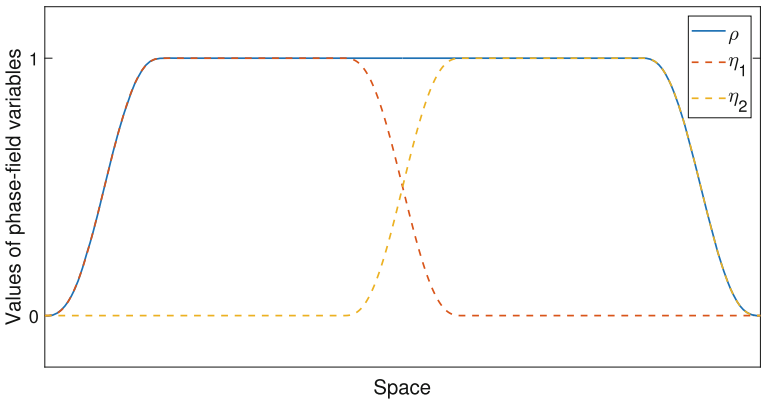

Fig. 1. Phase-field variables

According to [7], the total free energy of a heterogeneous system can be written as

$$F = \int f(\rho, \eta_1, ..., \eta_I) + \frac{1}{2}\beta_\rho |\nabla \rho|^2 + \frac{1}{2}\beta_\eta \sum_i |\nabla \eta_i|^2 d\Omega, \tag{1}$$

where f is a free local chemical energy density, β_ρ and β_η are gradient energy coefficients. The second term describes the impact of surface energy, and the third describes grain boundary energy's impact.

The evolution of ρ is given by the Cahn-Hilliard equation [7]. Mass density changes under the action of flow J, which is proportional to the gradient of the chemical potential μ (Fick's law [9]).

$$\frac{\partial \rho}{\partial t} = \nabla \cdot J \tag{2}$$

$$J = D \nabla \mu \tag{3}$$

$$\mu = \frac{\delta F}{\delta \rho} = \frac{\partial f}{\partial \rho} - \beta_\rho \Delta \rho \tag{4}$$

The Allen-Cahn equation describes the evolution of order parameters η_i [2].

$$\frac{\partial \eta_i}{\partial t} = -L \frac{\delta F}{\delta \eta_i} = -L\left(\frac{\partial f}{\partial \eta_i} - \beta_\eta \Delta \eta_i\right) \forall i, \tag{5}$$

where L is a constant related to grain boundary mobility.

Free local chemical energy density has the following form:

$$f(\rho, \eta_1, ..., \eta_I) = A\rho^2(1-\rho)^2 + B\Bigg(\rho^2 + 6(1-\rho)\sum_i \eta_i^2 - 4(2-\rho)\sum_i \eta_i^3 + 3\left(\sum_i \eta_i^2\right)^2\Bigg), \tag{6}$$

where A and B are surface and grain boundary energy constants. Function f has $I+1$ minima at points $\rho = 0,\ \eta_i = 0\ \forall i$ and $\rho = 1,\ \eta_i = 1,\ \eta_j = 0\ \forall j \neq i\ , 1 \leq i \leq I$ [35].

Substituting (6) into (2)–(5), we obtain:

$$\frac{\partial \eta_i}{\partial t} = -L(12B\eta_i(1-\rho-(2-\rho)\eta_i + \sum_j \eta_j^2) - \beta_\eta \Delta\eta_i)\ \forall i, \tag{7}$$

$$\frac{\partial \rho}{\partial t} = \nabla \cdot D\nabla\Bigg(2A\rho(1-\rho)(1-2\rho) + B(2\rho - 6\sum_i \eta_i^2 + 4\sum_i \eta_i^3) - \beta_\rho \Delta\rho\Bigg). \tag{8}$$

During the sintering, mass transport occurs by several diffuse paths.

1. Volume diffusion is the mass transport from within the grain.
2. Vapor diffusion is the mass transport through the pores.
3. Surface diffusion is the mass transport along the grain surface from the high-curvature areas to low-curvature ones.
4. Grain boundary diffusion is the mass transport along the boundary between grains.

The following form of diffusion coefficient allows taking into account all of these diffusion paths in phase-field terms:

$$D = D_{vol}\phi(\rho) + D_{vap}(1-\phi(\rho)) + D_{surf}\rho^2(1-\rho)^2 + D_{gb}\sum_{i<j}\eta_i\eta_j,$$
$$\phi(\rho) = \rho^3(10 - 15\rho + 6\rho^2). \tag{9}$$

$D_{vol}, D_{vap}, D_{surg}, D_{gb}$ are the constants related to material volume, vapor, surface, and grain boundary diffusivity, respectively.

To perform simulation, Eqs. (2) and (5) were discretized with respect to time by explicit forward Euler scheme with step τ. Spatial derivatives were discretized using central finite differences with grid step h for all directions.

3 Algorithm

If I is large, then for each order parameter η_i we define domain $\Omega_i = [X_{i1}^{min}, X_{i1}^{max}] \times [X_{i2}^{min}, X_{i2}^{max}] \times [X_{i3}^{min}, X_{i3}^{max}]$, which fulfills the condition $supp(\eta_i) \subseteq \Omega_i \subseteq \Omega$.

During simulation, grains change their shape and location. Thus, Ω_i should be changed too. Let us denote the minimal distance from grain i to planes bounding Ω_i as a $mindist_i$. Similarly, maximal distance is a $maxdist_i$.

The algorithm for tracking Ω_i consists of the following steps:

1. Initialization: domains Ω_i are chosen so that $mindist_i = maxdist_i = F_{start}, \forall i$.
2. Check: every T_r time steps, conditions $mindist_i > F_{min}, \forall i$ are checked.
3. Increasing: sizes of domains, for which condition $mindist_i > F_{min}$ failed, are increased so that $mindist_i = F_{start}$.
4. Total change: every T_{fr} time steps, all Ω_i change so that $mindist_i = maxdist_i = F_{start}, \forall i$.

Thus, four parameters $F_{min}, T_r, F_{start}, T_{fr}$ define the behavior of the algorithm. However, only two of them, F_{min} and T_r depend on model parameters. If we consider $\eta_i = 0.5$ as a grain surface, then F_{min} should not exceed half of the phase-field interface width. Otherwise, part of the interface will be outside of the domain. Restriction for the T_r depends on normal surface velocity. However, evaluating normal velocity for complex grains configuration is a difficult task. For one spherical grain with radius R, it is:

$$T_r < \frac{F_{min} R^2}{L\beta_\eta}, \tag{10}$$

because normal velocity has the following form [1]:

$$v_\eta = -L\beta_\eta \kappa_b, \tag{11}$$

where κ_b is the grain surface curvature.

4 Comparison Methods

Experiments are conducted in two variants. In the first of them, the evolution of order parameters η_i is computed in the whole domain Ω without tracking the subdomains. Let us denote this variant with subscript S. In the second variant with subscript T tracking algorithm is used.

One of the standard experiments for the sintering model is two spherical grains sintering [13,35]. During sintering, the neck growth between particles occurs. Sintering physics states that neck diameter to particles' diameter ratio has the following time dependence [35]:

$$\frac{X}{D} = Kt^n, \tag{12}$$

where n depends on the dominant diffusion mechanism. Thus, we can compare the dynamic of neck growth between solutions.

$$E_X(t) = \frac{|X_S(t) - X_T(t)|}{X_S(t)}. \tag{13}$$

Further, the solutions can be compared in l_∞-norm:

$$E_\rho(t) = \max_{x \in G} |\rho_S(x,t) - \rho_T(x,t)|,$$

where G is the set of grid nodes. Here we use absolute error instead of relative because of the following reasons: ρ varies in the range $[0,1]$, and the small interface shift cause enormous relative errors, making this measure unrepresentative.

Since we are primarily interested in changes in the sample's surface area, it is reasonable to compare this parameter of solutions.

$$E_A(t) = \frac{|A_S(t) - A_T(t)|}{|A_S(t)|}. \tag{14}$$

The surface area is computed with the Crofton formula [19] in the following way. Points a and b, are randomly chosen on the sphere which circumscribes the sample. Iterating along the line defined by a and b with the step $h/3$ (where h is the grid step), we count the number of intersections with the interface $\rho = 0.5$. The ρ value is trilinear interpolated at the points on the line. Assuming the sphere radius is R and M such experiments is performed with the number of intersections $\{N_1, ..., N_M\}$, than the surface area of the sample is approximately:

$$S \approx \frac{\sum_{i=1}^{M} N_i}{2M} \cdot 4\pi R^2. \tag{15}$$

Finally, the topology tools, such as Hausdorff distance and Betti numbers, allow us to estimate sample differences.

The Hausdorff distance between sets A and B is defined as:

$$d_H(A,B) = \max(\sup_{x \in A} \inf_{y \in B} |x - y|, \sup_{y \in B} \inf_{x \in A} |x - y|). \tag{16}$$

The diameter of set A is defined as:

$$diam(I) = \sup_{x,y \in A} |x - y|. \tag{17}$$

Since the solutions are defined in grid nodes, we can compute Hausdorff distance between sets of points $I_S(t) = \{x \in G | \rho_S(x,t) \geq 0.5\}$ and $I_T(t) = \{x \in G | \rho_T(x,t) \geq 0.5\}$ [32]. However, this approach's minimal possible distance (except zero) is equal to h, which is rather rough. Therefore we upscale grid G into grid G_u with step 0.2 h using trilinear interpolation and then calculate the relation of the interface shift to the diameter of the sample.

$$\begin{gathered} I_S(t) = \{x \in G_u | \rho_S(x,t) \geq 0.5\}, \\ I_T(t) = \{x \in G_u | \rho_T(x,t) \geq 0.5\}, \\ E_H(t) = \frac{d_H(I_S(t), I_T(t))}{diam(I_S(t))}. \end{gathered} \tag{18}$$

We can present the solution as a binary digital image, where nodes with value $\rho \geq 0.5$ correspond to the foreground and nodes with value $\rho < 0.5$ correspond to the background. The set of voxels with topology forms topological space. We define 26-connectivity on the foreground [28]. One of the informative characteristics of topology space is the sequence of Betti numbers $\{\beta_0, \beta_1, \beta_2 ...\}$; β_k is the rank of k–homology group [8]. In 3–dimensional space, all Betti numbers beginning with the third are zero. The first three present the following characteristics of topological space:

1. β_0 - the number of connected components,
2. β_1 - the number of through-holes,
3. β_2 - the number of closed voids.

Thus, we can exactly define if samples are different.

5 Numerical Experiments

To perform the simulation, we use two sets of parameters (Table 1). Both are aluminum oxide properties from [13] non-dimensionalized according to [1].

Table 1. Simulation parameters

Parameter	Two particles simulation	Packing simulation
A	4.933	7.733
B	0.667	0.267
β_ρ	17.5	25
β_η	12.5	5
L	0.203	0.129
D_{vol}	5.559×10^{-5}	3.103×10^{-5}
D_{vap}	2.779×10^{-5}	1.552×10^{-5}
D_{surf}	5.559×10^{-2}	3.103×10^{-2}
D_{gb}	5.559×10^{-2}	3.103×10^{-2}
$h_1 = h_2 = h_3 = h$	1	1
τ	0.05	0.05

All experiments were conducted at the Polytechnic Tornado supercomputer of Saint-Petersburg Polytechnic University equipped with CPU Intel Xeon E5 2697 v3 and GPU NVIDIA K40.

5.1 Simulation of Two Particles

The grid size of the two particles simulation (Fig. 2) is $120 \times 120 \times 200$ nodes. The radius of particles is equal to 40 spatial steps, which correspond to 1.25 μm. The simulations are performed during $5 \cdot 10^6$ time steps, corresponding to 4.5 h.

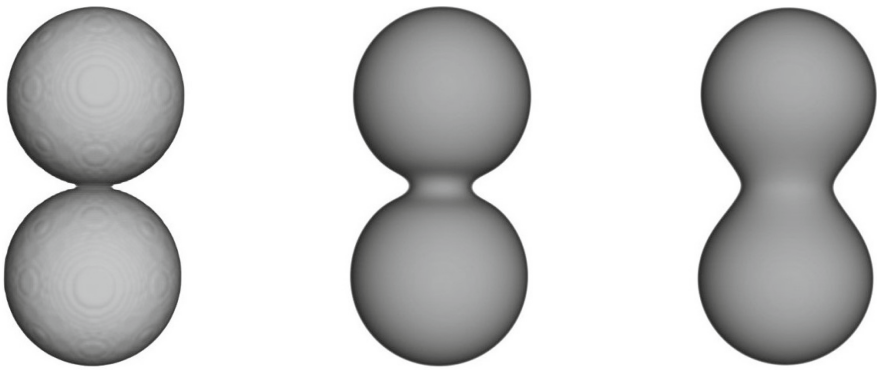

Fig. 2. Neck growth between two particles

We measure neck diameter 60 times at the steps $\{0, 1, 2, .., 9, 10, 20, .., 100, 200, ..., 5 \times 10^6\}$. Then, using the least square method, parameters of power dependence 19 are defined.

$$\frac{X}{D} = Kt^n + C. \tag{19}$$

Because grid resolution does not allow to define touch of the spheres exactly, the term C is added. The obtained value $n = 0.172$ corresponds to the estimation for grain boundary diffusion [11]. In Fig. 3, neck growth is shown for the solution obtained with the tracking of subdomains.

The value of $E_X(t)$ is less than 10^{-5}, E_ρ is less than 10^{-3}.

Two equal particles are in the equilibrium state. Therefore, the grain boundary does not move, and sizes change slightly. Thus, the only significant parameter of the algorithm is the F_{start}. However, obtained errors allow us to conclude that value $F_{start} = 10h_1$ provides good accuracy.

5.2 Packing Simulation

In this section, we present the results of the sintering simulation of ten packings consisting of 50 equal particles. Packings are prepared using the Lubachevsky-Stillinger algorithm [20]. The snapshots of the samples are saved 56 times at the steps $\{0, 1, 2, .., 9, 10, 20, .., 100, 200, ..., 1 \times 10^6\}$. The grid size is 110^3 nodes.

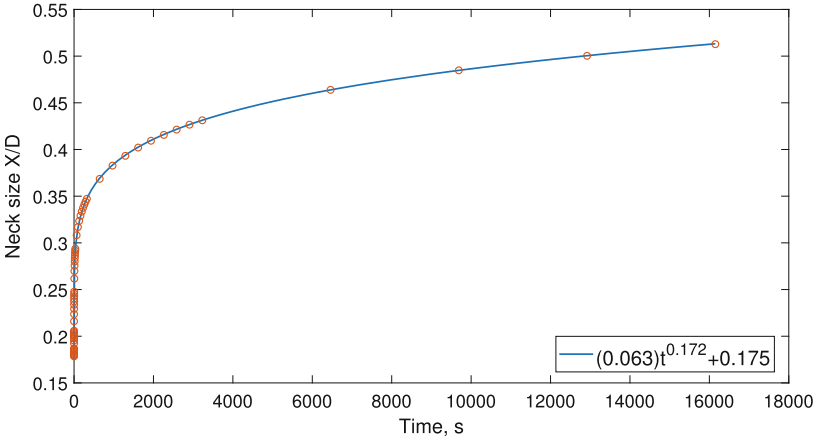

Fig. 3. Time dependence of neck diameter

The particles' radius equals 20 h, corresponding to 250 nm. The simulations are performed during 10^6 time steps, corresponding to 17.5 min.

We perform a simulation with and without tracking subdomains for each of the ten packings. In all experiments, the algorithm has the following parameters:

$$\begin{aligned} F_{min} &= 5\,\text{h}, \qquad T_r = 100\tau, \\ F_{start} &= 10\,\text{h}, \quad T_{fr} = 1000\tau. \end{aligned} \tag{20}$$

For most of the simulations, E_∞ is less than 0.01. The maximal value of $E_\infty = 0.037$ reaches for sample six at the middle of the simulation (Fig. 4 left). This peak also appears in the E_H graph (Fig. 4 right). Nevertheless, E_H has a maximum at the beginning of the simulation for the second sample, where E_∞ has a less significant peak. Even with the peaks, the maximal shift of the interface is less than 0.5% of the sample's diameter. Moreover, E_H values mainly lie on the line corresponding to the minimal possible distance 0.2 h specified by the computation method. The line has an incline because of the shrinkage of the sample during sintering, so the diameters decrease.

The obtained values of the E_A are less than 10^{-3}, which is in the range of Monte-Carlo method error. Thus the time dependence of E_A is not representative.

Then, in order to study the behavior of the algorithm, we perform six additional experiments with the 6th sample (Fig. 5), varying the algorithm parameters (Table 2). In Table 2 "Reference" row corresponds to the experiment without subdomains tracking.

Figures 6 and 7 (right) show that experiments 1, 2, and 5 have much larger error values than others. E_∞ reaches the value 0.25. E_A is less than 1%, but here accuracy of the Crofton formula allows us to differentiate changes in surface area. E_H is up to two percent, approximately 2 h interface shift. It means that in experiments 1 and 2 boundary of subdomains is too close to the interface,

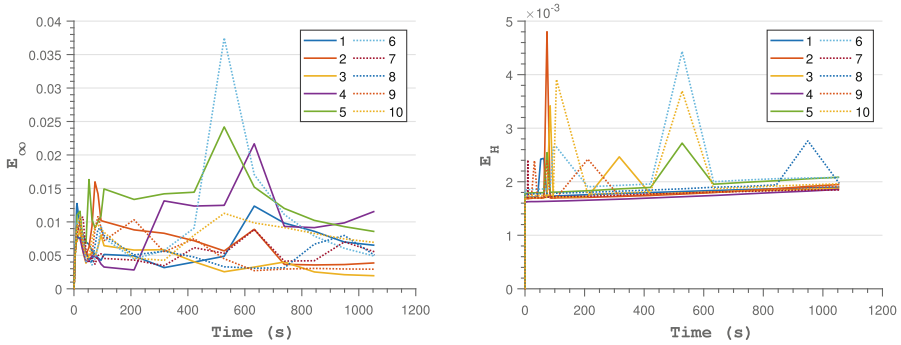

Fig. 4. Time-dependence of E_∞ (left) and E_H (right) for different experiments

Table 2. Algorithm parameters

Number	F_{min}	F_{start}	T_r	T_{fr}	Time (min)
1	3 h	6 h	100τ	1000τ	126
2	3 h	6 h	1000τ	10000τ	120
3	5 h	10 h	100τ	1000τ	133
4	5 h	10 h	1000τ	10000τ	124
5	5 h	10 h	10000τ	100000τ	146
6	10 h	20 h	1000τ	10000τ	220
7	10 h	20 h	10000τ	100000τ	160
Reference					2073

which significantly changes solutions. In experiment 5, domain resizing occurs very rarely, so the interface approaches too close to the boundary.

The sample consists of one connected component and has no void. Also, the sample does not split during the simulation, and voids do not appear. Therefore $b_0 = 1$ and $b_2 = 0$ constantly. The number of holes b_1 decreases during the simulation. At the beginning and end, the number is equal for all experiments. However, in all experiments except 6 and 7, b_1 slightly differs (Fig. 7 right). Graphs for experiments 3 and 4 (graph 4 overlaps the 3-d one in Fig. 7 right) do not feet to the reference in the one point. Graphs 1, 2, and 5 (graph 2 overlaps the 1-st one in Fig. 7 right) differ from the reference in several points. However, the difference in b_1 is equal to one. In spite of differences in b_1, we assume that the evolution of sample structure goes similarly; the cause of discrepancies in graphs are the small changes in the dynamic of pore collapse due to the different parameters of the tracking algorithm.

Thus, we can conclude that parameters 1, 2, and 5 are inappropriate for the current simulation. The four remaining sets of parameters are divided into two groups. Inside each of them, measured errors very close. So, we can choose the best parameters for performance reasons. Between parameters 3 and 4, the

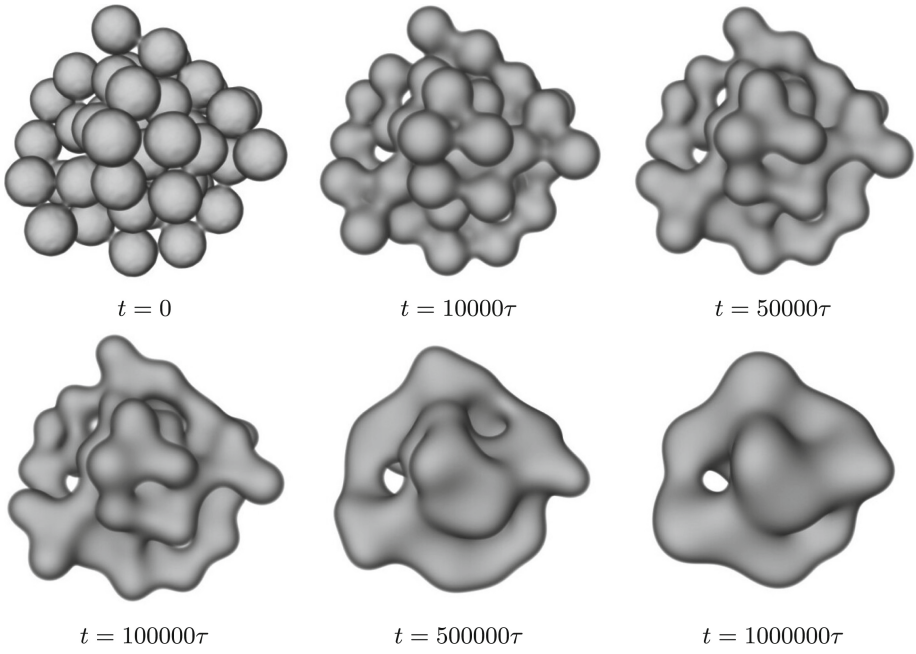

Fig. 5. Evolution of sample 6 (reference experiment)

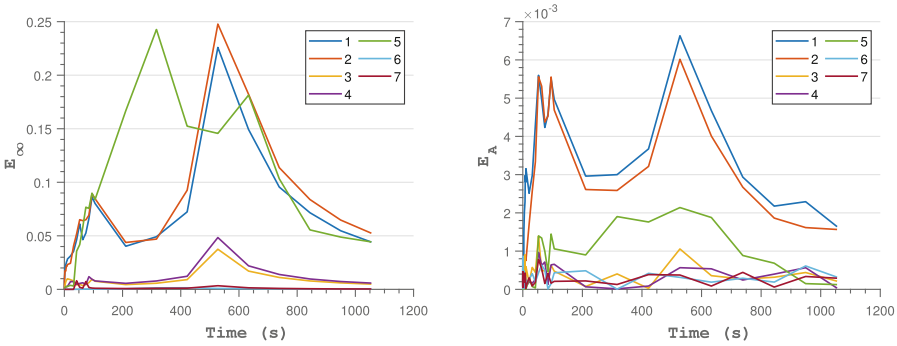

Fig. 6. Time-dependence of E_∞ (left) and E_A (right) for different algorithm parameters

winner is the fourth. Both experiments take a similar amount of memory (Fig. 8), but the fourth runs faster and has fewer errors than the third. There is no obvious winner between parameters 6 and 7. The seventh run faster but use more memory than the sixth. It seems reasonable to use parameters 6 at the beginning of the computation and then switch to parameters 7. The final conclusion, if the experiment is far from the memory limits, then parameters 6/7 are preferred. However, it is not true for the samples with a large number of grains and for the experiments on GPU without domain decomposition between several devices.

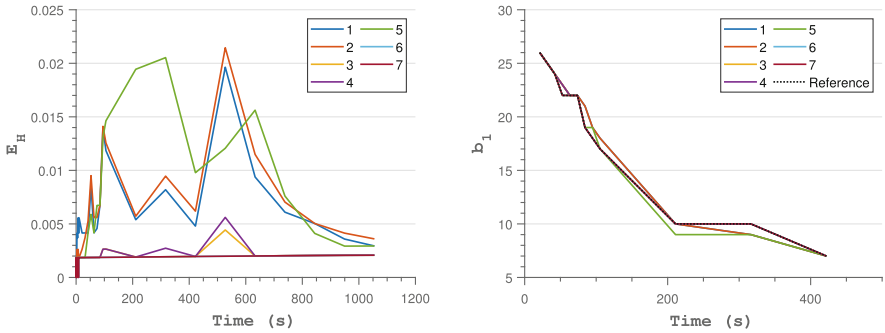

Fig. 7. Time-dependence of E_H (left) and b_1 (right) for different algorithm parameters

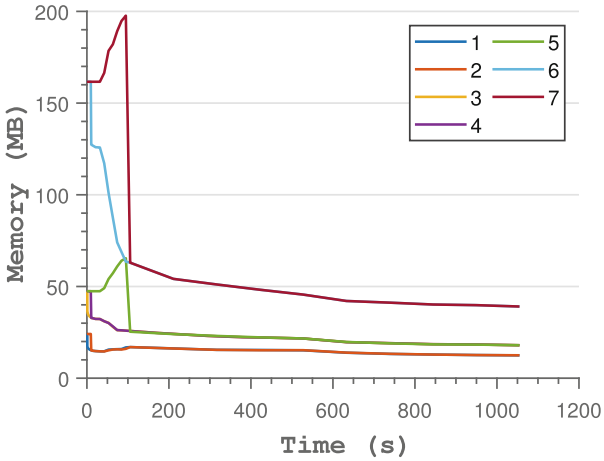

Fig. 8. Time-dependence of memory usage for storing order parameters for different algorithm parameters

6 Conclusion

The article presents a study of the qualitative properties of the algorithm for numerical simulation of sintering based on the system of Cahn-Hilliard and Allen-Cahn equations. The algorithm significantly decreases computational time by narrowing down the Allen-Cahn equations' evolution domains. However, the optimization alters obtained solutions. Besides common approaches, Hausdorff distance and Betti numbers are used to evaluate changes. Numerical experiments show that the solution has good quality if appropriate parameters are chosen. Parameters 3 (Table 2) seems to be the optimal decision. The analysis is performed for the single set of model parameters for packing consisting of 50 spherical grains with a radius of 10 h. However, the results can be generalized without new tests. First of all, the number of grains does not matter; the same

parameters can be used for any size of packing (but the amount of device memory should be considered). Secondly, the model parameters are divided into two groups related to surface energy and diffusion mobilities, respectively. Mobilities define the velocity of the interface, so we need to change parameters T_r and T_{fr} proportionally. Energy defines the contact angles, which do not relate much to the algorithm parameters. Also, by the energy parameters, the width of the phase-field interface is defined. For experiments with a large number of grains, small values (like 5 h or 3 h) are used. It is the phase-field method parameter, and it does not depend on material properties, so we do not need to choose parameters for a wide range of interface widths. Thirdly, according to Herring scaling law [29], larger grains sinter slower than the smaller ones, so the same parameter can be used for any grains larger than 10 h by accuracy reasons (by performance reasons, it can be changed). Finally, if the shape of the grain differs from the spherical, then the grain surface has higher curvature and moves faster than the surface of the spherical grain. Therefore, domains should be resized faster, but a rigorous study for this case has not been conducted.

Acknowledgements. Dmitry Prokhorov implemented the pahse-field method and developed algorithms for computing the characteristics of the grains packing digital representation under the support of the basic research program of the Russian Academy of Sciences contract no. FWZZ-2022-0022. Yaroslav Bazaikin analyzed the results under the institutional support of the Faculty of Science, Jan Evangelista Purkyně University in Ústí nad Labem, Czech Republic. Vadim Lisitsa performed a numerical experiments using "Polytechnic RSC Tornado" (SPBSTU, Russia) with the support of the Russian Science Foundation Grant No. 21-71-20003.

References

1. Ahmed, K., Pakarinen, J., Allen, T., El-Azab, A.: Phase field simulation of grain growth in porous uranium dioxide. J. Nuclear Mater. **446**, 90–99 (2014). https://doi.org/10.1016/j.jnucmat.2013.11.036
2. Allen, S., Cahn, J.: Ground state structures in ordered binary alloys with second neighbor interactions. Acta Metallurgica **20**(3), 423–433 (1972)
3. Aspert, N., Santa-Cruz, D., Ebrahimi, T.: Mesh: measuring errors between surfaces using the hausdorff distance. In: Proceedings. IEEE International Conference on Multimedia and Expo, vol. 1, pp. 705–708 (2002). https://doi.org/10.1109/ICME.2002.1035879
4. Bazaikin, Y., Derevschikov, V., Malkovich, E., Lysikov, A., Okunev, A.: Evolution of sorptive and textural properties of cao-based sorbents during repetitive sorption/regeneration cycles: part ii. modeling of sorbent sintering during initial cycles. Chem. Eng. Sci. **199**, 156–163 (2019). https://doi.org/10.1016/j.ces.2018.12.065, https://www.sciencedirect.com/science/article/pii/S0009250919300971
5. Bazaikin, Y., Malkovich, E., Prokhorov, D., Derevschikov, V.: Detailed modeling of sorptive and textural properties of CaO-based sorbents with various porous structures. Sep. Purif. Technol. **255**, 117746 (2021)
6. Bordia, R.K., Kang, S.J.L., Olevsky, E.A.: Current understanding and future research directions at the onset of the next century of sintering science and technology. J. Am. Ceram. Soc. **100**(6), 2314–2352 (2017). https://doi.org/10.1111/jace.14919

7. Cahn, J.W., Hilliard, J.E.: Free energy of a nonuniform system. i. interfacial free energy. J. Chem. Phys. **28**(2), 258–267 (1958). https://doi.org/10.1063/1.1744102
8. Edelsbrunner, H., Harer, J.: Computational topology: an introduction, January 2010. https://doi.org/10.1007/978-3-540-33259-6_7
9. Fick, A.: Ueber diffusion. Annalen der Physik **170**(1), 59–86 (1855)
10. Florin, N., Fennell, P.: Synthetic CaO-based sorbent for co2 capture, vol. 4, pp. 830–838 (2011). https://doi.org/10.1016/j.egypro.2011.01.126, https://www.sciencedirect.com/science/article/pii/S1876610211001287, 10th International Conference on Greenhouse Gas Control Technologies
11. German, R.M.: Sintering Theory and Practice. John Wiley & Sons Inc., New York (1996)
12. Hötzer, J., et al..: Large scale phase-field simulations of directional ternary eutectic solidification. Acta Materialia **93**, 194–204 (2015)
13. Hötzer, J., Seiz, M., Kellner, M., Rheinheimer, W., Nestler, B.: Phase-field simulation of solid state sintering. Acta Materialia **164** (2018). https://doi.org/10.1016/j.actamat.2018.10.021
14. Jettestuen, E., Friis, H.A., Helland, J.O.: A locally conservative multiphase level set method for capillary-controlled displacements in porous media. J. Comput. Phys. **428**, 109965 (2021)
15. K.A. Gadylshina, T.S. Khachkova, V.L.: Numerical modeling of chemical interaction between a fluid and rocks. Numer. Methods Program. (Vychislitel'nye Metody i Programmirovanie) **20**(62), 457–470 (2020). https://doi.org/10.26089/NumMet.v20r440, https://en.num-meth.ru/index.php/journal/article/view/1035
16. Kim, S.G., Kim, D.I., Kim, W.T., Park, Y.B.: Computer simulations of two-dimensional and three-dimensional ideal grain growth. Phys. Rev. E **74**, 061605 (2006)
17. Li, X., Huang, H., Meakin, P.: Level set simulation of coupled advection-diffusion and pore structure evolution due to mineral precipitation in porous media. Water Resour. Res. **44**(12), W12407 (2008)
18. Li, X., Huang, H., Meakin, P.: A three-dimensional level set simulation of coupled reactive transport and precipitation/dissolution. Int. J. Heat Mass Transf. **53**(13), 2908–2923 (2010)
19. Liu, Y.S., Yi, J., Zhang, H., Zheng, G.Q., Paul, J.C.: Surface area estimation of digitized 3d objects using quasi-monte carlo methods. Pattern Recognit. **43**, 3900–3909 (2010). https://doi.org/10.1016/j.patcog.2010.06.002
20. Lubachevsky, B.D., Stillinger, F.H.: Geometric properties of random disk packings. J. Stat. Phys. **60**, 561–583 (1990)
21. Marella, S., Krishnan, S., Liu, H., Udaykumar, H.S.: Sharp interface cartesian grid method i: an easily implemented technique for 3d moving boundary computations. J. Comput. Phys. **210**(1), 1–31 (2005)
22. Mittal, R., Iaccarino, G.: Immersed boundary methods. Annu. Rev. Fluid Mech. **37**(1), 239–261 (2005)
23. Moelans, N., Wendler, F., Nestler, B.: Comparative study of two phase-field models for grain growth. Comput. Mater. Sci. **46**, 479–490 (2009). https://doi.org/10.1016/j.commatsci.2009.03.037
24. Osher, S., Fedkiw, R.P.: Level set methods: an overview and some recent results. J. Comput. Phys. **169**(2), 463–502 (2001)
25. Peskin, C.S.: Flow patterns around heart valves: a numerical method. J. Comput. Phys. **10**, 252–271 (1972)

26. Pino, D., Julien, B., Valdivieso, F., Drapier, S.: Solid-state sintering simulation: surface, volume and grain-boundary diffusions. In: ECCOMAS 2012 - European Congress on Computational Methods in Applied Sciences and Engineering, e-Book Full Papers, September 2012
27. Poetschke, J., Richter, V., Gestrich, T., Michaelis, A.: Grain growth during sintering of tungsten carbide ceramics. Int. J. Refract. Metals Hard Mater. **43**, 309–316 (2014)
28. Prokhorov, D., Lisitsa, V., Khachkova, T., Bazaikin, Y., Yang, Y.: Topology-based characterization of chemically-induced pore space changes using reduction of 3d digital images. J. Comput. Sci. **58**, 101550 (2022)
29. Rahaman, M.N.: Sintering of Ceramics, 1 ed. CRC Press, Boca Raton (2007)
30. Smereka, P.: Semi-implicit level set methods for curvature and surface diffusion motion. J. Sci. Comput. **19**, 439–456 (2003)
31. Sotiropoulos, F., Yang, X.: Immersed boundary methods for simulating fluid-structure interaction. Prog. Aerosp. Sci. **65**, 1–21 (2014)
32. Taha, A.A., Hanbury, A.: An efficient algorithm for calculating the exact hausdorff distance. IEEE Trans. Pattern Anal. Mach. Intell. **37**(11) (2015). https://doi.org/10.1109/TPAMI.2015.2408351
33. Tanaka, H.: Sintering of silicon carbide and theory of sintering. J. Ceramic Soc. Jpn. **110**(1286), 877–883 (2002). https://doi.org/10.2109/jcersj.110.877
34. Tseng, Y.H., Ferziger, J.H.: A ghost-cell immersed boundary method for flow in complex geometry. J. Comput. Phys. **192**(2), 593–623 (2003)
35. Wang, Y.U.: Computer modeling and simulation of solid-state sintering: a phase field approach. Acta Materialia **54**(4), 953–961 (2006)
36. Zhang, J., Yue, P.: A level-set method for moving contact lines with contact angle hysteresis. J. Comput. Phys. **418**, 109636 (2020)
37. Zhang, R.J., Chen, Z.W., Fang, W., Qu, X.: Thermodynamic consistent phase field model for sintering process with multiphase powders. Trans. Nonferrous Metals Soc. China **24**, 783–789 (2014). https://doi.org/10.1016/S1003-6326(14)63126-5